

Characterizing and Understanding Divalent Adsorbates on Carbon Nanotubes with Ab Initio and Classical Approaches: Size, Chirality, and Coverage Effects

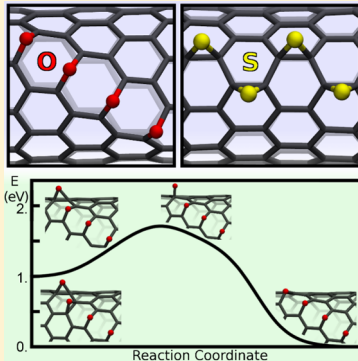
Jaap M H. Kroes,[†] Fabio Pietrucci,[†] Alessandro Curioni,[‡] and Wanda Andreoni^{*,†}

[†]Institut de Théorie des Phénomènes Physiques, Ecole Polytechnique Fédérale de Lausanne, 1015 Lausanne, Switzerland

[‡]IBM Research Zurich, 8803 Rüschlikon, Switzerland

Supporting Information

ABSTRACT: The study of oxygen chemisorption on single-walled carbon nanotubes generally relies on simple atomistic models and hence hampers the possibility to understand whether nanotube size or adduct concentration have a role in determining the surface–adsorbate interaction. Our large-scale DFT-based simulations show that structural and electronic properties as well as diffusion barriers strongly depend on both nanotube diameter and adsorbate concentration. Our atomistic models cover nanotube of different chirality with diameters from 0.6 to 1.5 nm and oxygen concentration from 0.1 to 1%. In particular, the tendency to cluster increases with concentration and stabilizes ether (ET) groups but affects hopping barriers only to a minor extent. Significant differences with graphene are found, also for 1.5 nm diameter nanotubes. Extension to species isoelectronic to oxygen reveals dissimilarities, and especially for sulfur that tends to form epoxides (EP), to diffuse more easily and to rapidly close the energy gap for increasing concentration. The relative ET–EP stability can be described in terms of the bare-bond curvature, a concentration-dependent chemical descriptor here introduced. Comparison of these DFT calculations—using different exchange-correlation functionals—and our additional investigation with a reactive force-field (ReaxFF) clarifies several similarities but also discrepancies between the predictions of the two schemes.



1. INTRODUCTION

Since their discovery in the early 1990s,¹ carbon nanotubes (CNTs) have attracted tremendous interest in view of their unique electronic and mechanical properties,² which continue to offer innovative solutions for nanotechnology applications.³ Intense research has been carried out, aimed at exploring their physicochemical behavior and in particular numerous calculations of any level of sophistication have described electronic, structural, mechanical, and dynamical properties of single-walled nanotubes (SWNTs).

Covalent sidewall functionalization⁴ is of special relevance for CNTs, because of their insolubility in water and most organic solvents. The need for covalent functionalization has stimulated widespread effort to understand chemisorption on the sidewalls and especially diverse addition reactions. In particular, oxygen-based functionalization, as well as the importance of oxygen as common attacking agent⁵ of a nanotube, has driven a number of investigations. The first attack to the carbon network by an oxygen atom can be understood on the basis of the fundamental CNT chemistry.⁶ For any chirality, the side-wall offers several inequivalent bridging sites. The bond between the two carbon atoms coordinated to oxygen can either undergo cleavage as in an ether (ET) group or be preserved as in an epoxide group (EP). In a number of cases, the occurrence of one or the other configuration on a given C–C bond can be predicted using simple geometrical descriptors relative to the

pristine tube.^{7,8} The same arguments apply to isoelectronic species, such as NH and CH₂. However, these arguments cannot decide on whether an ET or an EP configuration will be thermodynamically favored. The solution should come from ab initio calculations. Only recently,⁹ however, we have shown that at very low coverage atomic oxygen highly prefers ether configurations on the sidewall of a SWNT of ~1 nm diameter and that using atomistic models of small sizes severely affects the ET–EP energy differences.¹⁰ Moreover, with a joint computational (DFT-based) and experimental (scanning-tunneling spectroscopy (STS)) approach, we showed that metastable epoxides can act as effective kinetic traps⁹ for oxygen and give rise to characteristic impurity levels in the gap of the nanotube.

Here, we extend our DFT-PBE¹¹ calculations to nanotubes of larger diameter and to higher oxygen concentrations, thus determining CNT:nO probable configurations, their relative stability, binding energies, and hopping energy barriers. The latter are calculated also for oxygen isoelectronic species. In particular, our study includes sulfur chemisorption on which only very few computations are available,^{12,13} in spite of its recognized role in the growth of SWNTs.¹⁴ This set of results allows us to establish the power and limitations of simple

Received: August 2, 2014

chemical descriptors for the prediction of adsorbate configurations. In particular, we introduce the Mayer bond-order¹⁵ among these parameters.

Whereas nonempirical approaches are essentially limited to the single-oxygen attack, crucial problems concerning the effect of oxygen on the growth of nanotubes¹⁶ or on their mechanical and sensory properties have not been tackled yet with computations. Deterring factors might be size- and time-scale of realistic atomistic models and processes, respectively. Simulations based on reactive potentials could offer a viable approach. Indeed, this class of force-fields^{17–19} has, in principle, the possibility of capturing nontrivial chemistry and constitutes the most common choice for classical molecular dynamics and Monte Carlo simulations of carbon nanostructures.^{20,21} The validity of one of these schemes (AIREBO) for the description of hydrogen chemisorption on CNTs has been recently questioned.²² However, the success of the reactive force-field ReaxFF¹⁸ in the simulation of carbon nanotube growth, and also graphene oxide,²³ suggests that a careful analysis of its performance for oxygen adsorbates on CNTs could be useful at this stage. Following our first encouraging findings,⁹ here, we apply the ReaxFF potential to the same problems mentioned above, thus obtaining a detailed comparison with the DFT-PBE results.

Specifically, this work aims at providing an exhaustive answer to currently open questions: (i) How does the structure of the adsorbate develop with increasing oxygen concentration and how does the carbon pattern simultaneously change? Can one still predict the former on the basis of the bond pattern of the pristine nanotube alone? The result should clarify the effect of the adsorbate–adsorbate interaction or the influence of the deformation of the carbon network on successive chemisorption events. (ii) What is the size of the barriers that an oxygen has to overcome to transfer from one position to the other in the presence of other adsorbed oxygen atoms? (iii) How do the ET–EP competition and hopping barriers change from oxygen to its isoelectronic species and especially to sulfur? (iv) To what extent can electronic spectra near the band edges distinguish different adsorbate configurations? (v) How do the predictions of reactive force fields compare with those of DFT calculations?

2. METHODS

To represent the SWNTs, we consider atomistic models of ~300 to ~700 atoms in periodically repeated orthorhombic cells (a, b, b) with a between 34 and 41 Å and b between 21 and 30 Å. Ref 9 discussed the competition ET vs EP for a single-oxygen and showed, in particular, that a periodically repeated model of the (10,0) zigzag nanotube needed at least 200 atoms for convergence to be attained in the binding energy difference of the two configurations. This is the main origin of some quantitative discrepancies found with previous work on small models. The physics lies in the long-range disturbance induced on the π -electron system that implies slow convergence for the value of the EP energy. In extending our calculations to (slightly) larger oxygen concentration, the size of each model was chosen in such a way as to ensure convergence of the binding energies. For example, for 4 oxygens on the (10,0) CNT, the binding energy changes from 2.99 to 3.10 to 3.11 eV with increasing number of atoms in the unit cell, from 240 to 360 to 480. Therefore, all our calculations on the (10,0) CNT use a 360-atom unit cell.

Ab initio calculations are performed within the PBE¹¹ approximation for the exchange–correlation functional and the

plane-wave pseudopotential²⁴ scheme, as implemented in the CPMD code.²⁵ Part of the calculations were also repeated within the BLYP²⁶ and the hybrid PBE0²⁷ exchange–correlation functionals. In particular, we will report on the Kohn–Sham (KS) density of states (DOS) that refers to PBE0 calculations in the PBE-optimized geometries. The only remarkable difference from the PBE-DOS is the opening of the energy gap by 0.6–0.8 eV.

Calculations with the ReaxFF potential are based on the parametrization applied to simulate the catalytic growth of nanotubes²¹ and use the code in ref 28.

For the estimate of energy barriers, we use the nudged-elastic-band method (NEB).²⁹

For more details, one can see ref 9 and the Supporting Information of this article.

3. RESULTS AND DISCUSSION

3.1. Structure and Binding of Atomic n-Oxygen Adsorbates ($n = 1–4$). On the sidewall of a SWNT, oxygen is known to chemisorb on positions bridging the C–C bonds and to form either ET or EP configurations.⁶ This is clearly illustrated by the Electron Localization Function (ELF) in Figure 1. We have primarily considered ($n, 0$) CNTs that are

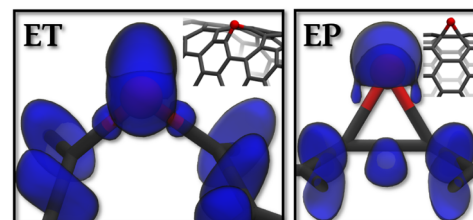


Figure 1. (10,0) CNT. Electron Localization Function (ELF) at (a) an ET (on the Z-bond) and (b) an EP (on the A-bond). The ELF level is 0.8.

characterized by the presence of only two types of C–C bonds, called zigzag (Z) and axial or armchair (A), and examined several possible oxygen arrangements. In particular, we were interested to study how the relative stability of ETs and EPs evolves with increasing diameter (D), from 0.6 to 1.5 nm, that is, for n increasing from 8 to 19, and for increasing concentration (n from 1 to 4). We also calculated chemisorption configurations on the (8,4), (6,5), and (12,10) CNTs, as representatives of other chiralities. There, three different types of C–C bonds are present.

Our investigation is restricted to semiconducting CNTs. We note that the diameter of the SWNTs obtained with the high pressure CO disproportionation (HiPco) process ranges between 0.8 and 1.2 nm.³⁰ We consider this range and also nanotubes with larger diameter (up to 1.5 nm), which allow for a comparison with graphene.

In the following, we characterize the energetics of the various systems with the binding energy (E_B) (per adduct A), defined as the opposite of the formation energy relative to the two separate fragments (at 0 K):

$$E_B(n) = (E(\text{CNT: } n\text{A}) - E(\text{CNT})) / n - E(\text{A}) \quad (1)$$

the energy loss (E_D) associated with the deformation of the nanotube structure induced by chemisorption (“deformation energy”):

$$E_D = E(\overline{\text{CNT}}) - E(\text{CNT}) \quad (2)$$

where $\overline{\text{CNT}}$ denotes the geometry after adsorption, and the aggregation energy E_C , namely the binding energy referred to that of an isolated adduct in its ground state:

$$E_C = E_B(n) - E_B(1) \quad (3)$$

As adducts, we consider oxygen, CH₂, NH, SiH₂, and S and refer the binding energy to their ground state that, with the exception of SiH₂, is a triplet. We have verified that there is a good agreement between the values obtained for the singlet-triplet splittings within the pseudopotential and all-electron calculations (see Table S1 in the Supporting Information).

For the (n,0) CNTs, the behavior of the KS energy gaps is consistent with previous calculations,³¹ and in particular, the PBE0 values decrease approximately as k/D for increasing diameter D beyond 1 nm, where $k = 1.4$ eV nm.

3.1.1. DFT Calculations. Structures and Binding Energies.

In the case of an isolated oxygen, the peculiar dependence of the chemisorption configuration on the specific C–C bond has been emphasized in many publications and can be understood on the basis of simple geometrical descriptors of the pristine tube.^{7,8} A specific discussion is postponed to section 3.1.2, where these arguments will be verified on oxygen chemisorption at higher concentration.

We find that on all (n,0) nanotubes of diameter $D < \sim 1.3$ nm ($n < 16$) the ET forms on the zigzag bond and is the thermodynamically favored configuration (see Figure 2a). This

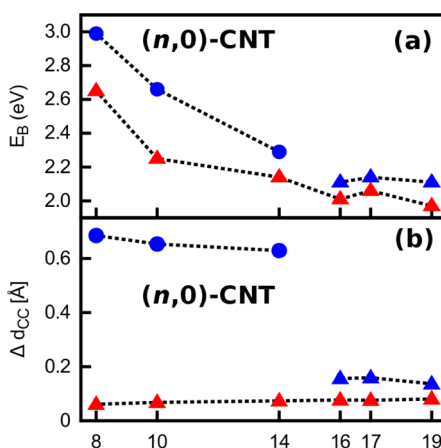


Figure 2. (n,0) CNTs. Variation of (a) the oxygen binding energy (eq 1,) and (b) the C–C bond-length on both Z (blue) and A (red) bonds, as a function of n . Circles and triangles refer to ETs and EPs, respectively. Lines through same symbols drawn as guide to the eye. Note the gap that marks the instability of ETs.

is also the case for the (8,4) and (6,5) CNTs, where bond cleavage takes place on one bond only. (see ref 9 for the former and Figure S1 in the Supporting Information for the latter). As shown in ref 9, an ET, although generating a longer-range strain field, does not perturb the conjugation on the hexagonal rings, whereas an EP implies more localized strain in the aromatic ring that induces a strong and long-range perturbation on the π states. This difference explains the higher binding energy of oxygen in an ET. For increasing diameter, the surface of the tube increasingly flattens so that, for $D > 1.3$ nm the zigzag bond can no longer sustain cleavage. In the limit-case of graphene only the EP is stable.^{32–34} Figure 2b shows the variation of the two C–C bond-lengths relative to the pristine

tube. As long as a significant difference exists between the two bonds, the most stable EP configuration is still the one with oxygen on the Z-bond, although it still generates more sizable (localized) strain on the sidewall (see Supporting Information Figure S2). In the (17,0) the corresponding deformation energy E_D (eq 2,) is 0.15 eV higher than with oxygen on the A-bond, and the binding energy E_B is 0.2 eV higher. These values should be compared to an E_D difference of 2.4 eV in the (10,0) where the Z-bond is broken and the ET is more strongly bound than the EP by 0.4 eV. Chiral nanotubes show the same trend, but bond cleavage is possible also for higher diameters (see section 3.1.2). Indeed in the (12,10) nanotube ($D = 1.5$ nm) an ET is still the lowest-energy configuration as in the (6,5) ($D = 0.75$ nm), and the ET–EP binding energy difference decreases sizably, from 1 eV (in (6,5) to 0.4 eV.

Figure 3 illustrates low-energy structures calculated for a (10,0) CNT and oxygen concentration increasing from 0.3 ($n =$

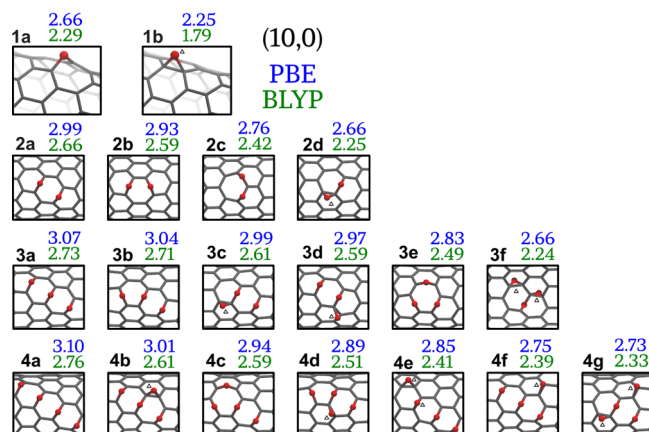


Figure 3. (10,0) CNT:nO ($n = 1\text{--}4$). Structures of chemisorbed oxygen for $n = 1$ and for cases with aggregation energy $E_C > 0$. Binding energies (in eV) refer to triplet oxygen. A small triangle indicates an EP.

1) to 1% ($n = 4$). (Others at higher energy are shown in Figure S3 of the Supporting Information.) The case $n = 1$ was studied in ref 9 and is here reported as reference. In each of the configurations shown in Figure 3 for $n = 2$, 3, and 4, the binding energy (E_B) per oxygen is higher than for $n = 1$ ($E_C > 0$ from eq 3). Therefore, oxygen atoms have a clear “tendency to cluster”. Clustering of ETs provides the configurations with higher E_B , especially when aligned. We find that if we consider only EPs, they also tend to cluster but even the preferred EP aggregates have much lower E_B than those composed of ETs only or those having mixed ET and EP populations (see Figure S3 in the Supporting Information). Regarding the (8,4) CNT, we considered the $n = 2$ case (Figure 4): two aligned ETs also correspond to the lowest-energy structure (2a) and two EPs (see e.g., (2f) in Supporting Information Figure S4) are highly disfavored.

Comparison in Figure 3 shows that BLYP predicts binding energies that are lower than the PBE values by ~15% but also that these GGA functionals closely agree in the prediction of the energy gain E_C associated with clustering and of the ranking of the different structures. Small differences are found in the predicted geometric characteristics (see Tables S2–S4 in the Supporting Information). PBE0 calculations on the PBE geometries resulted in a decrease of the binding energies of 0.4 to 0.5 eV. Geometry optimization with the PBE0 functional

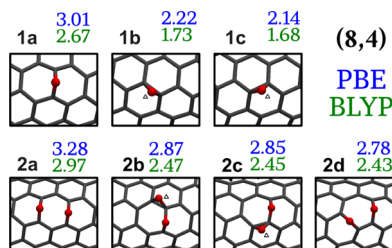


Figure 4. (8,4) CNT:nO. Structures of chemisorbed oxygen for $n = 1$ and for cases with aggregation energy $E_C > 0$. Notation as in Figure 3.

was only performed for the case of one oxygen on the (10,0) CNT and ended up in negligible changes relative to the PBE results, for example, the diameter reduced by less than 1% and the binding energies increased by 2%.

ETs continue to dominate on tubes of larger diameter than (10,0) and (8,4) ($D = 0.8$ nm) when more than one isolated oxygen chemisorbs. If we restricted our investigation to the case of one single oxygen discussed above, we would have predicted that CNTs with $D > 1.2$ nm do not allow bond opening and thus behave as expected for flat graphitic surfaces. However, the increase of concentration destabilizes EPs in favor of ETs. As illustrated in Figure 5 for (17,0), the lowest energy

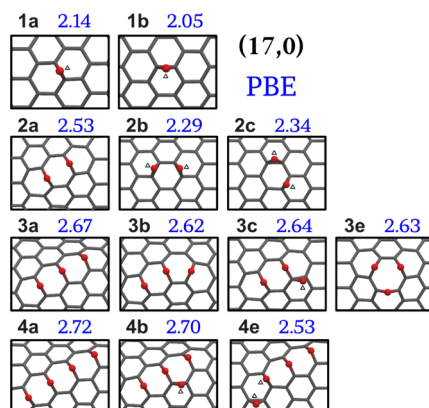


Figure 5. (17,0) CNT:nO ($n = 1-4$). Structures of chemisorbed oxygen for $n = 1$ and for selected configurations with aggregation energy $E_C > 0$. Notation as in Figure 3.

configuration of 2, 3, or 4 oxygens is again a chain of aligned ETs, with a sizable increase in binding energy per oxygen atom associated with clustering. The aggregation energy E_C is also higher for $n = 17$ than for $n = 10$. Figure 6 shows the pattern of

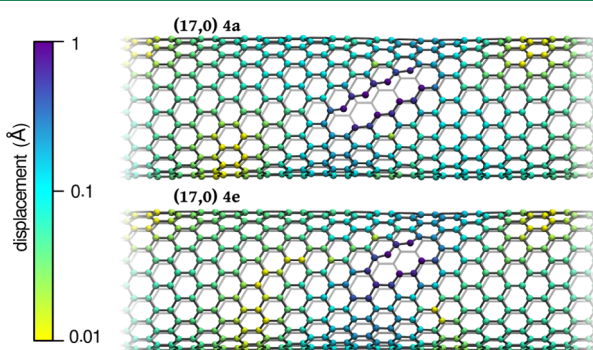


Figure 6. (17,0) CNT:4O. Displacements (in Å) of the carbon positions induced by oxygen chemisorption.

atom displacements in the adsorbate with four aligned ETs (4a) and in the one with three aligned ETs and one EP (4e). The presence of EPs in (4e) decreases the energy loss E_D due to structural deformation by 1.4 eV relative to (4a). In spite of it, in analogy with the $n = 1$ case on CNTs of higher curvature, the electronic contribution dominates the binding energy and here favors (4a) by 0.2 eV. For structural characteristics, see Supporting Information Table S5.

In conclusion, it should be emphasized that our findings are in agreement with the results of NEXAFS and infrared spectroscopies³⁵ on oxidized SWNTs that revealed higher relative stability for ETs.

Our study of nanotubes of higher diameters leads us naturally to discuss graphene as limiting case of a flat graphitic surface. Specific calculations of oxygen chemisorbed on graphene are strongly dependent on the model chosen for the latter.³²⁻³⁴ The lowest-energy structures for the $n = 2$ and $n = 3$ cases are predicted to consist of ETs with, however, different relative positions. For example, calculations on a $C_{54}H_{12}$ model for “a piece of graphene”³² predict that two aligned ETs (as in 2a of Figure 3) are the preferred configuration and that, in particular, this is 0.05 eV lower than one with two EPs on bonds in next-nearest-neighbor (NNN) positions (as in 2e of Supporting Information Figure S3). On the contrary, calculations using a periodic extended surface³⁴ claim that two NNN EPs (as in 2e) and three ETs on the same hexagonal ring (as in 3e of Figure 3) are the thermodynamically favored structures and, in particular, by 0.2 and 0.6 eV, respectively, than aligned ETs. As mentioned above, in the case of a (17,0) CNT (see Figure 5), we find again the aligned ETs as ground state configuration for $n = 2, 3$, and 4. Moreover, the EP pair in 2e is even higher in energy than two isolated oxygens, and the 3e is slightly higher than the ground state (by less than 0.1 eV). Given that ref 34 adopts the same PBE functional and a computational scheme very similar to ours, we could conclude that there is still a qualitative difference in the reactivity to oxygen of graphene and nanotubes of diameter ~ 1.3 nm. Therefore, simple extrapolation of our results—for example, for binding energies—to graphene is not possible.

Experiments on SiC-supported graphene³⁶ seem to suggest uniform oxygen distribution and “relatively long-range perturbation of the surface electronic structure around the chemisorbed oxygen”, which, as we have emphasized in ref 9 and will further show below, is characteristic of EP adsorbates.

Hopping Barriers. In ref 9, we have reported that, in the case of a single oxygen ($n = 1$ on the (10,0) CNT), this could be easily trapped in an EP configuration (metastable state) because of the high value of the barrier for hopping to the nearest-neighbor bond-bridging position, leading to an ET (from 1b to 1a in Figure 3). On the (10,0) tube, the energy barrier is as high as 0.8 eV in PBE, 0.6 eV in BLYP, and 0.7 eV in PBE0. On passing to the (14,0) CNT, in spite of a significant decrease in the ET–EP energy difference from 0.4 to 0.2 eV, we find that the PBE barrier increases by 0.1 eV. In both cases, the transition state corresponds to a configuration with oxygen on the on-top position, in which both Z and A bond-lengths are ~ 1.5 Å.

It is interesting to see how the barrier changes for an oxygen hopping from an EP to an ET in the presence of other oxygen atoms. In particular, we refer to the transitions from 2d to 2b and from 4e to 4a that involve one and two EPs respectively, adjacent to an ET. The paths of these transformations confirm the role of the on-top positions as transition states. In

particular, Figure 7 reveals a two-step mechanism, namely the oxygen detachment from one of the carbon atoms is preceded

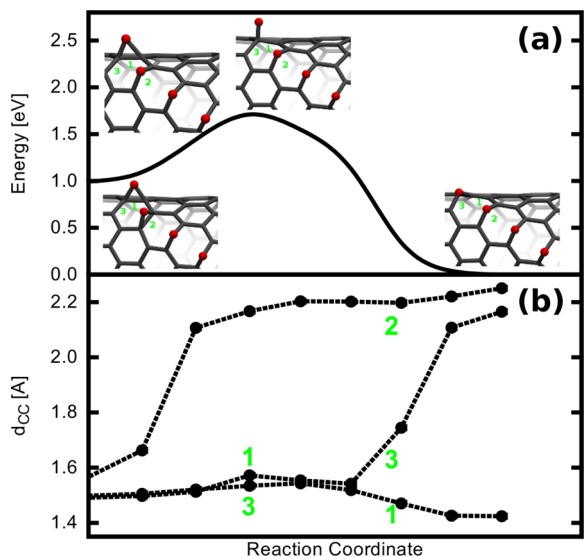


Figure 7. (10,0) CNT:4O—Transformation from 4e to 4a (see Figure 3). (a) Energy profile and sketch of the relevant structures; (b) variation of relevant distances.

by the EP to ET transformation on the zigzag bond. In both 2d to 2b and 4e to 4a transitions, the barriers are still of the order of 1 eV (Table 1). We can then conclude that also in the

Table 1. (10,0) CNT^a

I[conf]	F[conf]	ΔE^a
1b[EP]	1a[ET]	0.8
2b[ET]	2a[ET]	1.8 ^a
2d[EP]	2b[ET]	1.2
4e[EP]	4a[ET]	0.7

^aThis value refers to the higher barrier in the two-step mechanism shown in Figure 8. ^aEnergy barriers ΔE^* (in eV) for the hopping of one oxygen from an EP or ET in structure (I) to an ET in a lower-energy isomer (F).

presence of other oxygens in an ET or in clustered-aligned ETs, an additional oxygen can still be easily trapped in an EP. Other types of transformations, involving oxygen hopping between one ET to another ET on a different bond may imply even larger barriers. As an example, Figure 8 illustrates the transition from 2b to 2a, which goes through an intermediate (2f in Supporting Information Figure S3) involving an EP.

Oxygen migration on the sidewall of nanotubes has not received much attention so far. Still, the results of a DFT-PBE calculation has recently been published³⁷ for the 2d to 2a) transformation—also using the NEB method for the energy barriers—on small metallic nanotubes. The latter are not considered here so that a detailed comparison cannot be drawn. However, regarding the zigzag nanotube (9,0), we remark that the value reported for the energy difference of the two configurations is 0.43 eV, in agreement with what we found on the (10,0)-CNT. A significantly smaller barrier (about 0.6 eV), instead, can be deduced from the energy plot (Figure 5 in ref 37) but the path is not described. Given that the 2d to 2a) transition involves multiple steps, this specification is relevant.

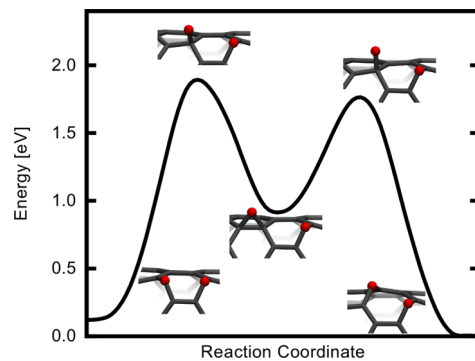


Figure 8. (10,0) CNT:2O—Transformation from 2b to 2a (see Figure 3). Energy profile and sketch of the relevant structures.

Kohn–Sham Electron States. In ref 9, we have shown that for the (10,0) CNT an ET leaves the Kohn–Sham (KS) density-of-states (DOS) at the band edges essentially unperturbed relative to the pristine tube whereas an EP generates a peculiar impurity level in the gap of the pristine tube. In the (8,4) and (6,5) nanotubes, an EP creates such a level only when located on one of the three inequivalent bonds: This was shown in ref 9 for the (8,4) and is here confirmed for the (6,5) and (12,10) CNTs (see Supporting Information Figure S5). A different scenario emerges from our results for the (17,0) CNT: here, as we have seen above, one oxygen is chemisorbed in an EP group both on the Z and on the A bond (Figure 5) but in neither case is a level seen in the gap of the pristine nanotube (Supporting Information Figure S6). On the other hand, the (16,0) CNT exhibits the same behavior as the (10,0) CNT.

This situation is only apparently complicated because it has a simple explanation. The appearance of an unoccupied level below the conduction band of the nanotube depends both on the spatial localization of the low-lying unoccupied levels of the nanotube and on the strength of the coupling with the chemisorbed atom. In the zigzag pristine nanotubes, the π -states can be classified as “delocalized over” one type of bond or the other. This is not always the case in the chiral ones, in which they can be “delocalized over” two out of three types of bond. Still the sequence depends on the characteristics of the tube. For example, in the zigzag class, it is governed by mod($n,3$) and thus is the same for (10,0) and (16,0) CNTs but is different for the (17,0) CNT. The electron densities corresponding to the HOMO and LUMO of the (10,0) CNT are shown in Figure 9: the former is on the Z-bonds, while the latter is on the A-bonds. This clarifies, for example, why the formation of an EP involving the A-bond as in 1(b) hybridizes with the LUMO and thus tends to localize and lower

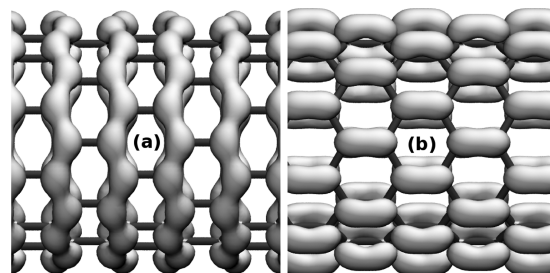


Figure 9. (10,0) CNT. Probability density corresponding to the HOMO (a) and LUMO (b). Isosurface = 0.0003 (au)⁻³.

the corresponding energy level. For a given atom, here oxygen, the coupling strength diminishes with increasing diameter of the tube. Accordingly, on passing from the (10,0) ($D = 0.79$ nm) to the (16,0) CNT ($D = 1.26$ nm), the LUMO-shift diminishes from 0.3 to 0.1 eV. On the contrary, in the (14,0) and (17,0) CNTs, the HOMO is on the A bonds whereas the LUMO is on the Z-bonds. Also, in the chiral ((6,5), (8,4), and (12,10)) nanotubes, the LUMO is on one specific bond (the one of lowest curvature again); in the former two, it is shifted by 0.25 eV when an oxygen is there chemisorbed (corresponding to the 1c structures in Figure 4 and Supporting Information Figure S1) and only by 0.06 eV in the (12,10).

For increasing concentration, clustered-ET configurations continue to elude spectra in the range of the gap of the CNT, as well as EPs on bonds of relatively high curvature (Z-sites in the ($n,0$) CNTs), whereas fingerprints of EPs on bonds of relatively low curvature can still be recognized. In analogy with the case of the (10,0) CNT,⁹ we find that in the (16,0) CNT:4O EPs on the A-sites continue to generate dispersionless bands in the gap (see Figure 10a and b), whereas in the (17,0) CNT:4O (see

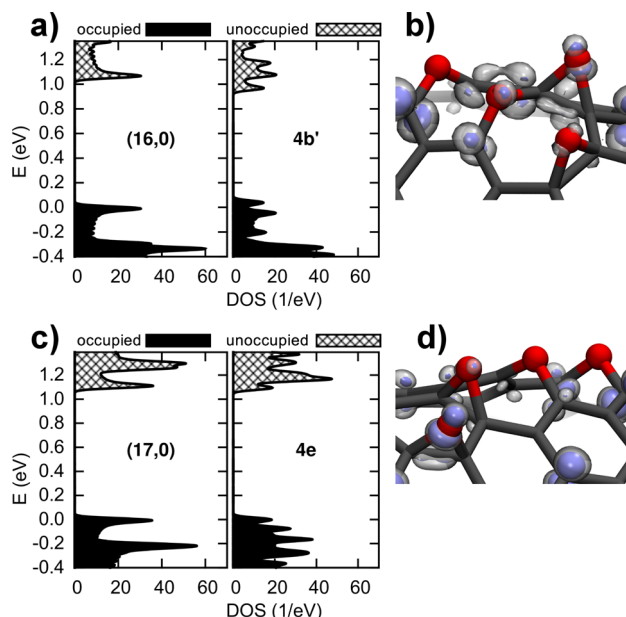


Figure 10. a) and c) DOS; b) and d) probability density corresponding to the LUMO in two adsorbate structures with mixed ET and EP populations. Isosurfaces = 0.0012, 0.002 (au)⁻³.

Figure 10c), due to weaker coupling, the EPs-related states are at the conduction band-edge (see, for example, Figure 10d for the 4e structure).

The effects of clustering on inequivalent positions is manifest in the distribution of the 2s-oxygen levels, about 3 eV below the rest of the valence bands. In the case of one oxygen, we find a clear separation—from 0.3 to 0.7 eV—between different configurations, depending on the specific nanotube. These values would thus correspond to isolated dispersed ET/EP groups. On the other hand, in adsorbates with 4O on the ($n,0$) CNTs, the four dispersionless bands cover an interval ranging from 0.8 eV for relatively distant groups (e.g., the four aligned ETs in the 4a structure) to 1.8–1.9 eV for mixed arrangements with two groups on adjacent bonds (bonding–antibonding splitting).

3.1.2. Chemical Descriptors. The chemical anisotropy of carbon nanotubes has attracted great interest and has resulted in the proposal of several descriptors for an a-priori understanding of their chemical behavior. In particular, the “directional curvature” (K_D) introduced in ref 8 has provided a guide for the understanding of the ET vs EP formation with [2 + 1] adducts, such as one oxygen or methylene, and also of the trends in reactivity and binding energies on the open bond. K_D refers to a pristine SWNT and is defined as in Figure 11, where

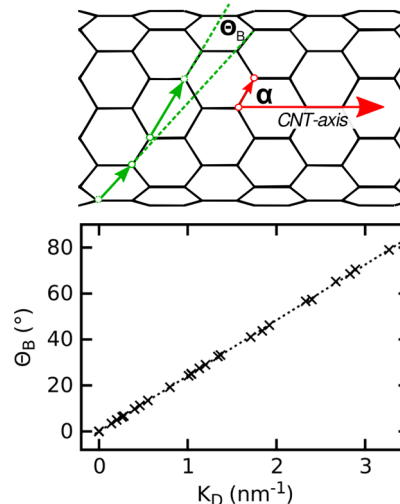


Figure 11. Curvature: definition of the “directional curvature” K_D and of the “bond curvature” Θ_B . K_D is defined as $(\sin \alpha)/D$, with D = the tube diameter.

the angle α is the angle between the bond direction and the CNT-axis. Therefore, in particular, for SWNTs of the same chirality, the value of K_D of the same type of bond (same α) changes only due to the change of the tube diameter. Here, we identify an angle Θ_B as in Figure 11, which is also related to the “curvature” of a given bond and can be more easily updated for any deformation of the SWNT structure. Therefore, since any chemisorption event involves a local deformation, we can use Θ_B —referred to the bare bond—to answer the question: “Given an adsorbate with a certain concentration, will a certain C–C bond open or not if an additional oxygen binds to it?” First, we considered an oxygen chemisorbed on a coronene molecule and bent it so that Θ_B would vary in the range from 0° to 80°. The transition from EP to ET is sharp and takes place at $\Theta_B = 32^\circ$. We then verified that in pristine tubes Θ_B and K_D are proportional (see Figure 11), and thus, there is no difference between their predictions for one [2 + 1] adduct (see Supporting Information Table S4). Our calculated limits are in the range 29°–33° for Θ_B (see Table 2)—in perfect agreement with the case of coronene—and between 1.13 and 1.37 nm⁻¹ for K_D . The latter is in excellent agreement with the result (1.5) obtained in ref 8, where different models, DFT functional and basis set were used.

Any structural parameter, be it a curvature or a bond-length, contains a complex information, with both geometrical and electronic ingredients. The notion of bond-order, instead, is directly related to the local electronic configuration. Therefore, we also examine to what extent its value—calculated according to Mayer’s prescription¹⁵—can be used to predict the response of a given bond to a [2 + 1] adduct. Indeed, one can expect that a lower BO is the symptom of a relatively higher tendency to

Table 2. One Oxygen on Semiconducting (*n*,0) Nanotubes^a

SWNT	bond	d_{cc}^i	Θ_B	BO	d_{cc}^f [conf.]	pred.
(8,0)	Z	1.434	57	1.21	2.119 [ET]	ET
	A	1.417	0	1.31	1.478 [EP]	EP
(10,0)	Z	1.428	46	1.23	2.082 [ET]	ET
	A	1.421	0	1.29	1.489 [EP]	EP
(14,0)	Z	1.427	33	1.24	2.056 [ET]	ET
	A	1.421	0	1.295	1.494 [EP]	EP
(16,0)	Z	1.425	29	1.25	1.581 [EP]	EP
	A	1.422	0	1.28	1.499 [EP]	EP
(17,0)	Z	1.426	27	1.25	1.585 [EP]	EP
	A	1.421	0	1.29	1.497 [EP]	EP
(19,0)	Z	1.424	24	1.25	1.561 [EP]	EP
	A	1.422	0	1.28	1.503 [EP]	EP

^aZ = zigzag; A = axial; d_{cc}^i and d_{cc}^f are the bond-lengths prior to chemisorption (pristine tube) and in the adsorbate configuration (ET or EP) respectively. Values (in Å) are from PBE calculations. pred = prediction based on limits defined for oxygen on coronene. Both Θ_B (in degrees) and BO refer to the pristine tube. Both give the same prediction for the final configuration.

cleavage. The above-mentioned calculation on coronene showed that EPs become unstable on a bond with Mayer BO lower than 1.25. Table 2 shows that, when using this limit, the predictions from the bare-bond order are correct for all the (*n*,0) nanotubes we have considered.

Tables 3 and 4 extend the above concepts to cases of multiple chemisorbed oxygens. With reference to Figure 3, we

Table 3. (10,0) CNT^a

FROM	bond	d_{cc}^i	Θ_B [pred]	BO [pred]	TO	d_{cc}^f [conf.]
1a	Z	1.449	53 [ET]	1.25 [ET]	2a	2.199 [ET]
1a	Z	1.447	53 [ET]	1.19 [ET]	2b	2.183 [ET]
1a	Z	1.415	58 [ET]	1.32 [EP]	2c	2.165 [ET]
1a	A	1.445	12 [EP]	1.28 [EP]	2d	1.470 [EP]
1b	Z	1.488	53 [ET]	0.98 [ET]	2d	2.268 [ET]
1b	Z	1.407	46 [ET]	1.37 [EP]	2e	1.547 [EP]
1b	A	1.409	0 [EP]	1.35 [EP]	2i	1.481 [EP]
1b	A	1.409	5 [EP]	1.35 [EP]	2j	1.482 [EP]
1b	Z	1.427	46 [ET]	1.23 [ET]	2k	2.073 [ET]
2a	Z	1.444	63 [ET]	1.28 [EP]	3a	2.180 [ET]
2a	Z	1.456	54 [ET]	1.15 [ET]	3b	2.200 [ET]
2a	A	1.385	14 [EP]	1.36 [EP]	3c	1.461 [EP]
2a	Z	1.414	55 [ET]	1.37 [EP]	3d	1.536 [EP]
2b	Z	1.446	53 [ET]	1.25 [ET]	3b	2.191 [ET]
2c	Z	1.430	53 [ET]	1.32 [EP]	3d	2.208 [ET]
2d	Z	1.469	55 [ET]	1.19 [ET]	3c	2.227 [ET]
2d	A	1.436	8 [EP]	1.31 [EP]	3f	1.524 [EP]
2i	Z	1.489	56 [ET]	0.995 [ET]	3f	2.280 [ET]
3a	Z	1.440	53 [ET]	1.29 [EP]	4a	2.165 [ET]
3c	Z	1.429	53 [ET]	1.36 [EP]	4b	2.177 [ET]

^aExample of the building up of the map in Figure 12a. Notation as in Table 2. Here, the initial (FROM) and final (TO) contain *n* and *n* + 1 oxygen atoms, respectively.

consider one bare-bond in a CNT:nO adsorbate and verify whether its Θ_B and BO values can be used to predict whether an ET or an EP will form if an additional oxygen is there chemisorbed ((*n* + 1)O adsorbate). The correlation between the final value of the C–C distance and the bare-bond curvature in Figure 12 confirms the predictive value of the latter. We have emphasized with empty symbols special

Table 4. (17,0) CNT^a

FROM	bond	d_{cc}^i	Θ_B	BO	TO	d_{cc}^f [conf.]
1a	Z	1.446	33 [ET]	1.16 [ET]	2a	2.194 [ET]
1a	Z	1.412	31 [EP]	1.285 [EP]	2b	1.557 [EP]
1a	A	1.409	4 [EP]	1.35 [EP]	2c	1.498 [EP]
1b	Z	1.407	30 [EP]	1.38 [EP]	2c	1.537 [EP]
2a	Z	1.445	37 [ET]	1.29 [EP]	3a	2.184 [ET]
2a	Z	1.456	35 [ET]	1.16 [ET]	3b	2.212 [ET]
2a	A	1.389	14 [EP]	1.35 [EP]	3c	1.471 [EP]
2b	Z	1.443	33 [ET]	1.17 [ET]	3b	2.194 [ET]
2b	A	1.404	8 [EP]	1.45 [EP]	3e	2.211 [ET]
2c	Z	1.398	33 [ET]	1.46 [EP]	3e	2.242 [ET]
3a	Z	1.441	38 [ET]	1.30 [EP]	4a	2.171 [ET]
3a	A	1.405	18 [EP]	1.335 [EP]	4b	1.500 [EP]

^aNotation as in Table 3.

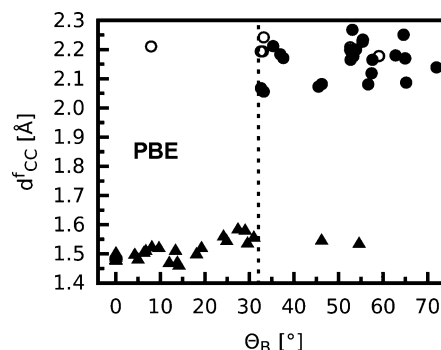


Figure 12. C–C distance in the ET or EP groups as a function of the angle Θ_B , which refers to the bond before chemisorption. Triangles and open circles represent EPs and ETs, respectively. These symbols represent the configurations calculated for oxygen adsorbates on (*n*,0), (8,4), (6,5), (12,10) nanotubes discussed in the text and also the (6,6) bond of fullerene (highest value of Θ_B).

circumstances for which the prediction fails because under the addition of an extra oxygen the local structure changes so that other bonds—near the one targeted—open or close, or, in other words, the final configuration is the result of concerted or multistep bond reconstructions. Only few failures are visible: the transformations from 1b to 2e and from 2a to 3d. These cases correspond to “extreme” values of the BO (1.37) and show the predominance of the electronic factor in determining whether cleavage takes place.

On the contrary, the BO, which is highly sensitive to variations in the distribution of the π states, appears to fail more frequently than Θ_B as concentration increases. However, these “failures” can be rationalized. For example, in 2a and 3a the BO of the Z-bond aligned with the ETs increases beyond the coronene limit, so that one would not predict an easy cleavage as it happens in 3a and 4a. This increase is more dramatic in 3c, where the Z-bond is near an EP (and two ETs). The threshold could be easily modified from coronene to the CNT domain. On the other hand, failures in correspondence to “extreme” values of the bond curvature can be expected: the structural constraint is then prevailing in the ET vs EP competition. This is the case of the (6,5) CNT in which an ET forms on a high-BO bond (Table 5) where also the variation of BOs with bond-lengths is anomalous. Indeed, on passing from zigzag to chiral nanotubes, it is important to note that structural constraints are more severe and, in particular, do not allow the higher-BO bonds to relax. This explains also the case of the (8,4) CNT

Table 5. Examples on Chiral CNTs^a

FROM	bond	d_{α}^i	Θ_B [pred]	BO [pred]	TO	d_{α}^f [conf.]
(8,4)						
n = 0	1	1.426	57 [ET]	1.28 [EP]	1a	2.081 [ET]
	2	1.428	25 [EP]	1.22 [ET]	1b	1.545 [EP]
	3	1.425	6 [EP]	1.26 [ET]	1c	1.505 [EP]
1a	1	1.441	65 [ET]	1.31 [EP]	2a	2.170 [ET]
1b	1	1.426	55 [ET]	1.27 [EP]	2b	2.234 [ET]
1b	1	1.404	59 [ET]	1.395 [EP]	2d	2.178 [ET]
1c	1	1.487	65 [ET]	1.01 [ET]	2c	2.251 [ET]
(6,5)						
n = 0	1	1.426	65 [ET]	1.29 [EP]	1a	2.087 [ET]
	2	1.424	19 [EP]	1.23 [ET]	1b	1.521 [EP]
	3	1.424	13 [EP]	1.24 [ET]	1c	1.512 [EP]
(12,10)						
n = 0	1	1.424	33 [ET]	1.275 [EP]	1a	2.068 [ET]
	2	1.422	10 [EP]	1.25 [EP]	1b	1.521 [EP]
	3	1.420	7 [EP]	1.265 [EP]	1c	1.511 [EP]

^aNotation as in Table 3.

(Table 5). For large-enough sizes, the Θ_B -BO consistency is expected to recover. However, this is not the case yet for the (12,10) CNT ($D = 1.50$ nm) as shown in Table 5.

3.1.3. ReaxFF Force-Field: A Comparison. When applied to determine the stable structures of chemisorbed oxygen, ReaxFF presents a serious problem: an arrangement of isolated oxygens on on-top positions is the ground state (Figure 13). On the

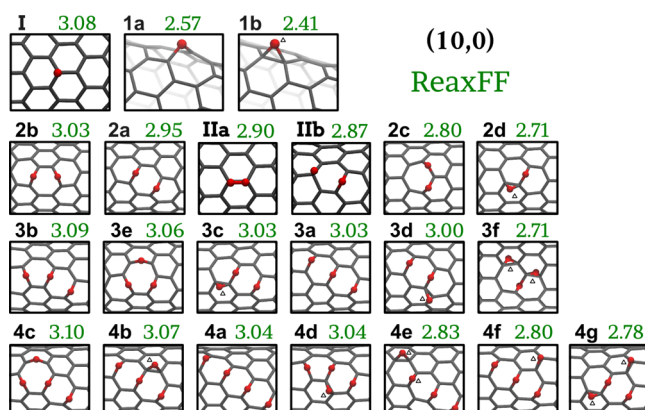


Figure 13. (10,0) CNT:nO structures from ReaxFF. Notation as in Figure 3 apart from roman numerals that refer to cases with oxygen on on-top positions. Note: $d(O-O) = 1.25$ Å in IIa. Note that $E(O) = 0$ in this scheme.

contrary, these structures are unstable in our—and previous¹⁰—ab initio calculations. We notice that in ReaxFF clustering of on-top oxygens is disfavored; for example, pairing on ortho positions (Ia) corresponds to a loss of 0.2 eV per atom.

However, if we only compare the geometrical characteristics and the relative stability of ETs vs EPs, the agreement with the ab initio description is rather good. This can be argued from the plot of binding energies in Figure S7 (in the Supporting Information) and through comparison of Figure 13 and Figure 3. More precisely, ETs are predicted to be more stable than EPs and the relative ranking is similar although EPs are less disfavored. For the geometrical details, we refer the reader to Tables S6–S9 in the Supporting Information. We remark “spurious” values for the C–C distances (from 1.6 and 1.8 Å,

which lie between those of an sp^2 C–C bond (as in the EP) and of an ET.

We also analyzed the validity of the Θ_B and BO. ReaxFF values (Tables S10–S13, Supporting Information) as chemical descriptors, and, in particular, whether the bare-bond curvature correlates well with the result of chemisorption (Figure 14b).

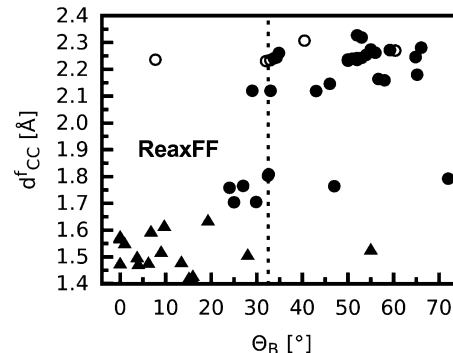


Figure 14. Same as Figure 12 for ReaxFF.

We note that the BO values intrinsic to this scheme scale well with the Mayer BOs, as can be seen in Figure S8, Supporting Information. This correspondence allows one to classify final configurations with “spurious” distances as ETs. Moreover, calculations on coronene suggest not too different ranges for the EP-ET transition: 32.5° for Θ_B and between 1.270 and 1.265 for the BO. However, a number of discrepancies can be recognized, and especially the lower performance of the bare-bond curvature and the frequent lack of consistency between the two descriptors also for the (n,0) CNTs.

Comparing hopping paths and barriers is meaningless because the TS configurations in DFT are minima of the potential energy surface of the ReaxFF potential. These can then act either as sink or intermediates also for transitions from EP.

3.2. CH₂, NH, SiH₂, and Sulfur Compared with Oxygen. We refer to our results in Table 6 and denote as ET and EPs the open and 3-member rings, respectively.

Chemisorption of one CH₂ or NH group on nanotubes has often been considered at the same time as oxygen (see ref 10c and 7). We have considered both functional groups on the (10,0) CNT and found that, as expected, the ET on the zigzag bond is strongly favored over the EP on the axial bond as in the

Table 6. (10,0) CNT^a

	BL(Z)	E_B (Z)	BL(A)	E_B (A)	Z-A	ΔE^*
O	2.082	2.66	1.489	2.25	0.41 [1.11]	0.8
NH	2.124	2.09	1.512	1.57	0.40/0.50 ^b [1.28]	1.4
CH ₂	2.113	2.93	1.539	2.44	0.49 [1.33]	1.9
SiH ₂	1.666	0.62	1.557	0.52	0.10 [0.89]	0.4
S	1.561	1.22	1.498	1.32	-0.10 [-]	0.5

^aBond-length (BL) (in Å) of Z and A bonds after chemisorption and corresponding binding energy E_B (in eV), and energy barrier ΔE^* (in eV) for the hopping of a [2 + 1] adduct from the metastable to the ground state. Note that in all cases, but sulfur, Z corresponds to the ground state and A to the metastable state. Also the Z–A energy difference is reported explicitly to allow for comparison with previous calculations—in brackets—performed for the (8,0) CNT (ref 10c).

^bThe two values correspond to the two adjacent Z bonds that in this case are inequivalent.

case of oxygen and also by a comparable amount ($\Delta(\text{ET}-\text{EP}) \simeq 0.5$ eV). Also, the electronic structure close to the band-edges closely resembles the case of oxygen chemisorption. In particular, the EP introduces a midgap level a few tenths of an eV below the bottom of the conduction band of the pristine tube (at about 0.2 and 0.1 eV for CH_2 and NH, respectively).

A more sizable difference is found for the values of the binding energies and of the energy barriers for the hopping from the metastable EP to the ET state (Table 6). Previous calculations for the (8,0) CNT, using relatively small hydrogen-terminated models, (see ref 10c) predict values 2–3 times larger for $\Delta(\text{ET}-\text{EP})$ for O, CH_2 , and NH. Our value for the (8,0) CNT is 0.4 eV as for the (10,0) CNT (see Figure 2a). Again, we attribute this discrepancy to the slow convergence of the binding energy as a function of the model size.⁹ However, the trend is the same.

SiH_2 does not behave in a similar way as its counterpart methylene (Table 6): It still tends to preferentially sit on the zigzag bond and to stretch it but not as strongly as to break it, as can be argued from the ELF in Figure 15. The more

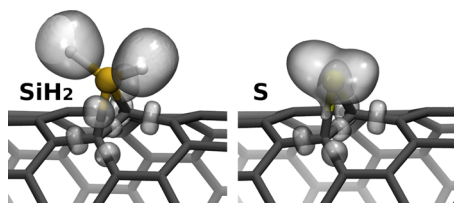


Figure 15. (10,0) CNT: SiH_2 /S. Electron Localization Function (ELF) (0.8) at the EP on the Z-bond.

delocalized nature of the electron wave functions of the adduct strongly decreases the binding energy and makes it less sensitive to the C–C bond specificity ($\Delta(\text{ET}-\text{EP})$ is only 0.1 eV to be compared to 0.9 eV in ref 10c). This tendency is clearer in the case of sulfur (Table 6), which is bound to the nanotube in the form of an EP on both C–C bonds (Figure 15). We also notice that sulfur has a larger binding energy on the axial bond. An increase of concentration confirms the fact that the thermodynamically favored structures are EPs only (Figure 16). Clear preference for clustering also emerges from Figure 16, with alternating patterns on the A sites. Z-bonds are

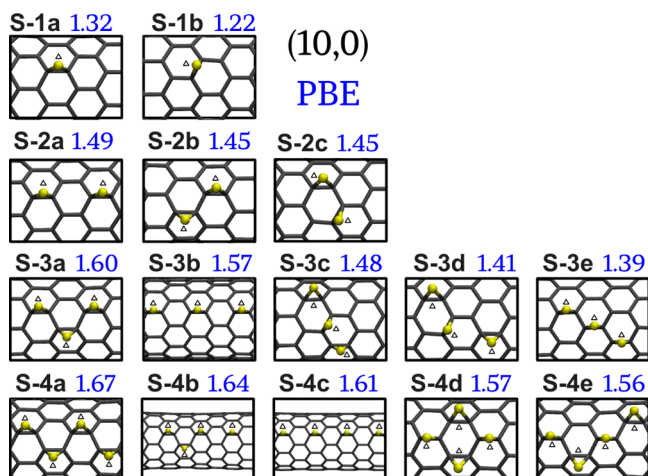


Figure 16. (10,0)CNT:nS ($n = 1$ –4). Structures and binding energies E_B (in eV) referred to triplet sulfur. A small triangle indicates an EP.

disfavored for $n > 1$ and can either be preserved or cleaved upon chemisorption, depending on concentration (see Supporting Information Figure S9). PBE0 calculations on the PBE geometries resulted in a decrease of the binding energies of ~ 0.2 eV.

Comparison with oxygen EPs shows that the bond-angle reduces from about 60° (61° – 66°) by at least 10° (45° – 49°) in the sulfur 3-member rings—an obvious size effect—whereas the pyramidalization angles of the carbon atoms are still about 10° and the deformation energy E_D is lower than 1 eV (e.g., 0.8 eV in both S-1a and S-1b (Figure 16) to be compared to 0.7 eV in 1b (Figure 3)). However, the binding energy is much weaker as found in previous model calculations^{12,13} and in agreement with indications from experiment.³⁸ Details of these structures are reported in Supporting Information Table S14.

From the above, it is clear that the idea that an adsorbate structure is determined only by the pristine CNT is no longer valid. It worked as long as only first-row atoms were involved in the bonding with carbon. Now we learn that, if we want to use K_D or Θ_B or BO as predictors, their limiting values must be adjusted to the characteristics (e.g., size) of the headatom. Calculations of S adsorbed on coronene would predict a less sharp correlation between Θ_B and the “final” C–C distance than the one observed for oxygen: 3-member rings are stable up to $\sim 60^\circ$ whereas the open-ring configuration is stable from $\sim 69^\circ$. The critical BO range is instead limited between 1.13 and 1.15. Clearly, a much higher curvature (what we called “extreme” for the case of oxygen) is necessary for bond cleavage to happen and also a sizably lower BO. The few cases here computed for sulfur on nanotubes indicate that thioethers could form on bonds of high but somewhat smaller curvature ($\Theta_B \sim 55^\circ$) than in coronene (see Supporting Information Table S15).

Both SiH_2 and sulfur must overcome lower barriers than their counterparts to hop from one bond to the other (Table 6). The case of SiH_2 is more interesting because the molecule undergoes two transformations as illustrated in Supporting Information Figure S10.

Both 3s- and 3p-levels of the sulfur atom resonate with the valence band of the nanotube and induce changes delocalized over several electron volts. In particular, a non-negligible mixing and a shift of the highest-occupied molecular orbitals of the nanotube is observed. The characteristic midgap level associated with the EP at the A-site appears also in this case (see Figure 17). The increase in concentration adds other such

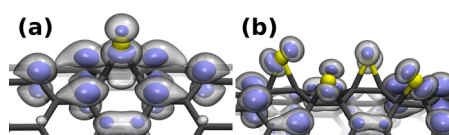


Figure 17. (10,0) CNT:nS. Probability density corresponding to the LUMO in the (a) S-1a and (b) S-4a structures (see Figure 16). Isosurfaces = 0.008, 0.002 (au)⁻³.

levels and may tend to rapidly close the gap (see Figure 18). We remark that these results were calculated with the PBE0 functional and that in PBE the gap would close already for the (10,0):4S CNT.

4. CONCLUSIONS

The extensive calculations presented above allow us to answer the questions that we posed in the Introduction.

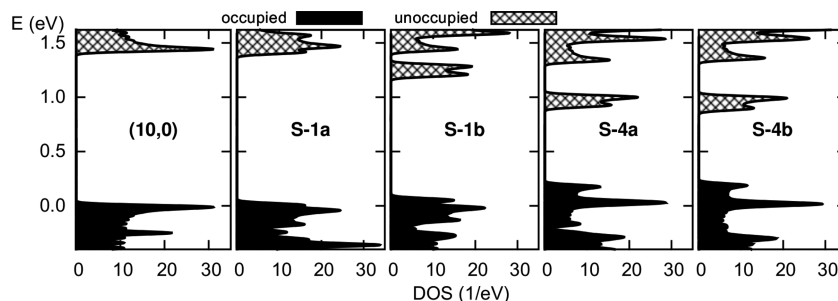


Figure 18. (10,0) CNT:nS. Kohn–Sham DOS for $n = 1$ and $n = 4$.

With increasing concentration, we observe an increasing tendency of oxygen atoms to cluster, with ETs energetically preferred and thus an increasing structural deformation of the nanotube. Metastable EP configurations act as kinetic traps. They tend to avoid this deformation of the sidewall but generate ring strain (local loss of conjugation). Progressive changes of the neighboring bonds induced by the presence of other chemisorbed oxygens do not allow to predict whether an additional oxygen will be chemisorbed in an ET or an EP on the basis of the characteristics of the pristine nanotube alone. An update of the bare-bond curvature, which accounts for the modifications induced by nearby chemisorption, still provides good predictions on possible bond cleavage, at least in the coverage-range considered here, unless other local modifications of the bond pattern take place.

Functional groups that are isoelectronic to oxygen behave in a similar way if the headatom belongs to the first row of the periodic table. On passing from oxygen to sulfur and from CH_2 to SiH_2 , instead, the opening of the C–C bonds becomes improbable apart from cases of high curvature attained in chiral nanotubes of diameter smaller than 0.8 nm. Given the preference for EPs, sulfur preserves the closed carbon rings but may induce sizable changes in the electronic properties of the nanotube.

Comparison of the outcome of the reactive force field ReaxFF and DFT-GGA shows similar results for the ET–EP competition but reveals that the most probable arrangement predicted by ReaxFF at low temperature is independent of concentration and consists of oxygen atoms in on-top sites and dispersed on the sidewall. On the contrary, on-top positions are unstable sites in the DFT-GGA and in the hybrid PBE0 functional frameworks. Therefore, ReaxFF and DFT descriptions of the reaction dynamics are bound to be very different. Any attempt to improve on the reactive potential parametrization—which appears mandatory for reliable process simulations—can benefit from the database here produced.

Comparison with similar but partial calculations of a few oxygens on graphene models still shows important differences between graphene and nanotubes of 1.3 nm diameter. In particular, oxygen chemisorption does not seem to provide a way to unzip the sidewall of SWNTs: EPs are effective traps for oxygen (hopping from an EP corresponds to high energy barriers) and ETs—especially clustered—are stable.

In conclusion, we remark that, provided specific catalysts are devised, hopping of a divalent chemisorbed atom or functional group between an EP and an ET configuration could provide a mechanism for the control and tuning of bond-cleavage on the sidewall of a nanotube, in alternative to the on-site bond-switch induced by adduct rotation suggested in ref 39 for bulky [2 + 1] adducts such as dichlorocarbene.

ASSOCIATED CONTENT

Supporting Information

Results on geometrical characteristics of the adsorbate structures presented in the main text, on other higher-energy configurations, electronic structures, energy profiles for diffusion, predictions from the chemical descriptors here discussed, and further comparison between ReaxFF and DFT-PBE results. All these results are cited in the main text. This material is available free of charge via the Internet at <http://pubs.acs.org>.

AUTHOR INFORMATION

Corresponding Author

*Email: wanda.andreoni@epfl.ch.

Notes

The authors declare no competing financial interest.

ACKNOWLEDGMENTS

This research was funded by Nano-Tera.ch, a program of the Swiss Confederation, evaluated by the SNSF. The computational work was supported by a grant from the Swiss National Supercomputing Centre, CSCS, under project ID 245.

REFERENCES

- (1) (a) Iijima, S. Helical microtubules of graphitic carbon. *Nature* **1991**, *354*, 56–58. (b) Iijima, S.; Ichihashi, T. Single-shell carbon nanotubes of 1-nm diameter. *Nature* **1993**, *363*, 603–605. (c) Bethune, D. S.; Klang, C. H.; De Vries, M. S.; Gorman, G.; Savoy, R.; Vazquez, J.; Beyers, R. Cobalt-Catalysed Growth of Carbon Nanotubes with Single-Atomiclayer Walls **1993**, *363*, 605–607.
- (2) Jorio, A., Dresselhaus, G., Dresselhaus, M., Eds. *Carbon Nanotubes: Advanced Topics in the Synthesis, Structure, Properties, and Applications*; Springer: Berlin and Heidelberg, 2008.
- (3) (a) Franklin, A.; Luisier, M.; Han, S.-J.; Tulevski, G.; Gignac, L.; Lundstrom, M.; Haensch, W. Sub-10 nm carbon nanotube transistor. *Nano Lett.* **2012**, *12*, 758–762. (b) Shulaker, M. M.; Hills, G.; Patil, N.; Wei, H.; Chen, H.-Y.; Wong, P. H.-S.; Mitra, S. Carbon nanotube computer. *Nature* **2013**, *501*, 526–530. (c) Park, S.; Vosguerichian, M.; Bao, Z. A review of fabrication and applications of carbon nanotube film-based flexible electronics. *Nanoscale* **2013**, *5*, 1727–1752.
- (4) (a) Banerjee, S.; Hemraj-Benny, T.; Wong, S. S. Covalent surface chemistry of single-walled carbon nanotubes. *Adv. Mater.* **2005**, *17*, 17–29. (b) Balasubramanian, K.; Burghard, M. Chemically functionalized carbon nanotubes. *Small* **2005**, *1*, 180–192. (c) Peng, X.; Wong, S. S. Functional covalent chemistry of carbon nanotube surfaces. *Adv. Mater.* **2009**, *21*, 625–642. (d) Benjamin, G.; Syrgiannis, Z.; Backes, C.; Graupner, R.; Hauke, F.; Hirsch, A. Carbon nanotube sidewall functionalization with carbonyl compounds-modified birch conditions vs the organometallic reduction approach. *J. Am. Chem. Soc.* **2011**, *133*, 7985–7995. (e) Hodge, S. A.; Bayazit, M. K.; Coleman, K. S.; Shaffer, M. S. P. Unweaving the rainbow: A review of the relationship between

- singlewalled carbon nanotube molecular structures and their chemical reactivity. *Chem. Soc. Rev.* **2012**, *41*, 4409–4429.
- (5) (a) Ajayan, P. M.; Ebbesen, T. W.; Ichihashi, T.; Iijima, S.; Iijima, K.; Hiura, H. Opening carbon nanotubes with oxygen and implications for filling. *Nature* **1993**, *362*, 522–525. (b) Collins, P.; Bradley, K.; Ishigami, M.; Zettl, A. Extreme oxygen sensitivity of electronic properties of carbon nanotubes. *Science* **2000**, *287*, 1801–1804.
- (6) Niyogi, S.; Hamon, M. A.; Hu, H.; Zhao, B.; Bhowmik, P.; Sen, R.; Itkis, M. E.; Haddon, R. C. Chemistry of Single-Walled Carbon Nanotubes. *Acc. Chem. Res.* **2002**, *35*, 1105–1113.
- (7) Zheng, G.; Wang, Z.; Irle, S.; Morokuma, K. Origin of the linear relationship between CH₂/NH/O-SWNT reaction energies and sidewall curvature: Armchair nanotubes. *J. Am. Chem. Soc.* **2006**, *128*, 15117–15126.
- (8) (a) Li, J.; Jia, G.; Zhang, Y. Bond-curvature effect of sidewall [2 + 1] cycloadditions of single-walled carbon nanotubes, a new criterion to the adduct structures. *Chem. Mater.* **2006**, *18*, 3579–3584. (b) Li, J.; Jia, G.; Zhang, Y. Chemical anisotropies of carbon nanotubes and fullerenes caused by the curvature directivity. *Chem.—Eur. J.* **2007**, *13*, 6430–6436.
- (9) Kroes, J. M. H.; Pietrucci, F.; Curioni, A.; Jaafar, R.; Gröning, O.; Andreoni, W. Atomic oxygen chemisorption on carbon nanotubes revisited with theory and experiment. *J. Phys. Chem. C* **2013**, *117*, 1948–1954.
- (10) (a) Dag, S.; Guelseren, O.; Yildirim, T.; Ciraci, S. Oxygenation of carbon nanotubes: Atomic structure, energetics, and electronic structure. *Phys. Rev. B* **2003**, *67*, 165424–165433. (b) Barone, V.; Heyd, J.; Scuseria, G. Effect of oxygen chemisorption on the energy gap of chiral single-walled carbon nanotubes. *Chem. Phys. Lett.* **2004**, *389*, 289–292. (c) Chen, Z.; Nagase, S.; Hirsch, A.; Haddon, R. C.; Thiel, W.; Schleyer, P. v. R. Side-wall opening of single-wall carbon nanotubes (SWCNTs) by chemical modification: A critical theoretical study. *Angew. Chem.* **2004**, *116*, 1578–1580.
- (11) (a) Perdew, J. P.; Burke, K.; Ernzerhof, M. Generalized gradient approximation made simple. *Phys. Rev. Lett.* **1996**, *77*, 3865–3868. (b) Perdew, J. P.; Burke, K.; Ernzerhof, M. Erratum. *Phys. Rev. Lett.* **1998**, *80*, 891–894.
- (12) Lu, X.; Sun, C.; Li, F.; Chen, H.-M. Selected absorption behavior of sulfur on single-walled carbon nanotubes by DFT. *Chem. Phys. Lett.* **2008**, *454*, 305–309.
- (13) Denis, P. A.; Faccio, R. Theoretical characterization of thioepoxidated single wall carbon nanotubes. *Chem. Phys. Lett.* **2008**, *460*, 486–491.
- (14) McNicholas, T. P.; Ding, L.; Yuan, D.; Liu, J. Density enhancement of aligned single-walled carbon nanotube thin films on quartz substrates by sulfur-assisted synthesis. *Nano Lett.* **2009**, *9*, 3646–3650.
- (15) (a) Bridgeman, A. J.; Cavigliasso, G.; Ireland, L. R.; Rothery, J. The Mayer bond order as a tool in inorganic chemistry. *J. Chem. Soc., Dalton Trans.* **2001**, 2095–2108. (b) Mayer, I. Bond order and valence indices: A personal account. *J. Comput. Chem.* **2007**, *28*, 204–221.
- (16) Koh, A. L.; Gidcumb, E.; Zhou, O.; Sinclair, R. *Observations of Carbon Nanotube Oxidation in an Aberration-Corrected Environmental Transmission Electron Microscope* **2013**, *7*, 2566–2572.
- (17) Brenner, D. W.; Shenderova, O. A.; Harrison, J. A.; Stuart, S. J.; Ni, B.; Sinnott, S. B. A second-generation reactive empirical bond order (REBO) potential energy expression for hydrocarbons. *J. Phys.: Cond. Matt.* **2002**, *14*, 783–802.
- (18) van Duin, A. C. T.; Dasgupta, S.; Lorant, F.; Goddard, W., III ReaxFF a reactive force field for hydrocarbons. *J. Phys. Chem. A* **2001**, *105*, 9396–9409.
- (19) Los, J. H.; Ghiringhelli, L. M.; Meijer, E. J.; Fasolino, A. Improved long-range reactive bond-order potential for carbon. I. Construction. *Phys. Rev. B* **2005**, *72*, 214102–214115.
- (20) (a) Bernholc, J.; Brenner, D.; Buongiorno Nardelli, M.; Meunier, V.; Roland, C. Mechanical and electrical properties of nanotubes. *Annu. Rev. Mater. Res.* **2002**, *32*, 347–375. (b) Hu, Y.; Shenderova, O. A.; Hu, Z.; Padgett, C. W.; Brenner, D. W. Carbon nanostructures for advanced composites. *Rep. Prog. Phys.* **2006**, *69*, 1847–1875. (c) Neyts, E.; van Duin, A. C. T.; Bogaerts, A. Changing chirality during single-walled carbon nanotube growth: A reactive Molecular Dynamics/Monte Carlo study. *J. Am. Chem. Soc.* **2011**, *133*, 17225–17231. (d) Lindsay, L.; Broido, D. A. Optimized Tersoff and Brenner empirical potential parameters for lattice dynamics and phonon thermal transport in carbon nanotubes and graphene. *Phys. Rev. B* **2010**, *81*, 205441–205446. (e) Neyts, E. C.; van Duin, A. C. T.; Bogaerts, A. Insights in the plasma-assisted growth of carbon nanotubes through atomic scale simulations: Effect of electric field. *J. Am. Chem. Soc.* **2011**, *134*, 1256–1260. (f) Neyts, E. C.; Ostrikov, K.; Han, Z. J.; Kumar, S.; van Duin, A. C. T.; Bogaerts, A. Defect healing and enhanced nucleation of carbon nanotubes by low-energy ion bombardment. *Phys. Rev. Lett.* **2013**, *110*, 065501–065504. (g) Kroes, J. M. H.; Akhukov, M. A.; Los, J. H.; Pineau, N.; Fasolino, A. Mechanism and free-energy barrier of the type-57 reconstruction of the zigzag edge of graphene. *Phys. Rev. B* **2011**, *83*, 165411–165418. (h) Colonna, F.; Fasolino, A.; Meijer, E. C. Graphitization of single-wall nanotube bundles at extreme conditions: Collapse or coalescence route. *Phys. Rev. B* **2013**, *88*, 165416–165420.
- (21) Nielson, K.; van Duin, A. C. T.; Osgaard, J.; Deng, W.-Q.; Goddard, W. A., III Development of the ReaxFF reactive force field for describing transition metal catalyzed reactions, with application to the initial stages of the catalytic formation of carbon nanotubes. *J. Phys. Chem. A* **2005**, *109*, 493–499.
- (22) Andreoni, W.; Curioni, A.; Kroes, J. M. H.; Pietrucci, F.; Gröning, O. Exohedral hydrogen chemisorption on a carbon nanotube: The clustering effect. *J. Phys. Chem. C* **2012**, *216*, 269–275.
- (23) Huang, L.; Seredych, M.; Bandosz, T. J.; van Duin, A. C. T.; Lu, X.; Gubbins, K. E. Controllable atomistic graphene oxide model and its application in hydrogen sulfide removal. *J. Chem. Phys.* **2013**, *139*, 194707–194715.
- (24) Troullier, N.; Martins, J. L. Efficient pseudopotentials for plane-wave calculations. *Phys. Rev. B* **1991**, *43*, 1993–2006.
- (25) CPMD, Copyright IBM Corp. 1990–2014, Copyright MPI für Festkörperforschung Stuttgart 1997–2001, <http://www.cpmd.org>.
- (26) (a) Becke, A. D. Density-functional exchange-energy approximation with correct asymptotic behavior. *Phys. Rev. A* **1988**, *38*, 3098–3100. (b) Lee, C.; Yang, W.; Parr, R. G. Development of the Colle-Salvetti correlation-energy formula into a functional of the electron density. *Phys. Rev. B* **1988**, *37*, 785–789.
- (27) Adamo, C.; Barone, V. Toward reliable density functional methods without adjustable parameters: The PBE0 Model. *J. Chem. Phys.* **1999**, *110*, 6158–6170.
- (28) <http://www.engr.psu.edu/adri/ReaxffEntry.aspx>.
- (29) Mills, G.; Jonsson, H. Quantum and thermal effects in H₂ dissociative adsorption: Evaluation of free energy barriers in multidimensional quantum systems. *Phys. Rev. Lett.* **1994**, *72*, 1124–1127.
- (30) Bronikowski, M. J.; Willis, P. A.; Colbert, D. T.; Smith, K. A.; Smalley, R. E. Gas-phase production of carbon single-walled nanotubes from carbon monoxide via the HiPco process: A parametric study. *J. Vac. Sci. Technol. A* **2001**, *19*, 1800–1805.
- (31) Sun, G.; Kurti, J.; Kertesz, M.; Baughman, R. Variations of the geometries and band gaps of single-walled carbon nanotubes and the effect of charge injection. *J. Phys. Chem. B* **2003**, *107*, 6924–6931.
- (32) Li, J.-L.; Kudin, K. N.; McAllister, M. J.; Prud'homme, R. K.; Aksay, I. A.; Car, R. Oxygen-driven unzipping of graphitic materials. *Phys. Rev. Lett.* **2006**, *96*, 176101–176104.
- (33) Yan, J.-A.; Chou, M. Y. Oxidation functional groups on graphene: Structural and electronic properties. *Phys. Rev. B* **2010**, *82*, 125403–125410.
- (34) Sun, T.; Fabris, S. Mechanisms for oxidative unzipping and cutting of graphene. *Nano Lett.* **2012**, *12*, 17–21.
- (35) Kuznetsova, A.; Popova, I.; Yates, J. T., Jr.; Bronikowski, M. J.; Huffman, C. B.; Liu, J.; Smalley, R. E.; Hwu, H. H.; Chen, J. G. Oxygen-containing functional groups on single-wall carbon nanotubes: NEXAFS and vibrational spectroscopic studies. *J. Am. Chem. Soc.* **2001**, *123*, 10699–10704.

- (36) Hossain, M. Z.; Johns, J. J.; Bevan, K. H.; Hunter, J. K.; Liang, Y. T.; Yoshimoto, S.; Mukai, K.; Koitaya, T.; Yoshinobu, J.; Kawai, M.; Lear, A. M.; Kesmodel, L. L.; Tait, S. L.; Hersam, M. C. Chemically homogeneous and thermally reversible oxidation of epitaxial graphene. *Nat. Chem.* **2012**, *4*, 305–309.
- (37) Liu, B.; Jiang, H.; Krasheninnikov, A. V.; Nasibulin, A.; Ren, W.; Liu, C.; Kauppinen, E.; Cheng, H.-M. Chirality-dependent reactivity of individual single-walled carbon nanotubes. *Small* **2013**, *9*, 1379–1386.
- (38) Curran, S. A.; Cech, J.; Zhang, D.; Dewald, J. L.; Avadhanula, A.; Kandadai, M.; Roth, S. Thiolation of carbon nanotubes and sidewall functionalization. *J. Mater. Res.* **2006**, *21*, 1012–1018.
- (39) (a) Lee, Y.-S.; Marzari, N. Cycloaddition functionalizations to preserve or control the conductance of carbon nanotubes. *Phys. Rev. Lett.* **2006**, *97*, 116801–116804. (b) Li, E.; Marzari, N. Improving the electrical conductivity of carbon nanotube networks: A first-principles study. *ACS Nano* **2011**, *5*, 9726–9736. (c) Li, E.; Poilvert, N.; Marzari, N. Switchable conductance in functionalized carbon nanotubes via reversible sidewall bond cleavage. *ACS Nano* **2011**, *5*, 4455–4465.

■ NOTE ADDED IN PROOF

Further tests using the ReaxFF parameters from the 2008 paper by Chenoweth, K., et al. (Chenoweth, K.; van Duin, A. C. T.; Persson, P.; Cheng, M. J.; Oxgaard, J.; Goddard, W. A. Development and application of a ReaxFF reactive force field for oxidative dehydrogenation on vanadium oxide catalysts. *J. Phys. Chem. C* **2008**, *112*, 14645–14654) have shown better agreement with DFT: similar trends as the 2005-parametrization, a reduced agreement on the binding energies and enhanced stabilization of the ETs. More importantly, the on-top positions are still local energy minima but highly disfavored relative to ETs and EPs. Further and detailed comparison will be published elsewhere.